1   **The Pathogenicity of SARS-CoV-2 in hACE2 Transgenic Mice**

2

3   Linlin Bao[†,1], Wei Deng[†,1], Baoying Huang[†,2], Hong Gao[†,1], Jiangning Liu[†,1], Lili Ren[3],

4   Qiang Wei[1], Pin Yu[1], Yanfeng Xu[1], Feifei Qi[1], Yajin Qu[1], Fengdi Li[1], Qi Lv[1], Wenling

5   Wang[2], Jing Xue[1], Shuran Gong[1], Mingya Liu[1], Guanpeng Wang[1], Shunyi Wang[1], Zhiqi

6   Song[1], Linna Zhao[1], Peipei Liu[2], Li Zhao[2], Fei Ye[2], Huijuan Wang[2], Weimin Zhou[2], Na

7   Zhu[2], Wei Zhen[2], Haisheng Yu[1], Xiaojuan Zhang[1], Li Guo[3], Lan Chen[3], Conghui Wang[3],

8   Ying Wang[3], Xinming Wang[3], Yan Xiao[3], Qiangming Sun[4], Hongqi Liu[4], Fanli Zhu[4],

9   Chunxia Ma[4], Lingmei Yan[4], Mengli Yang[4], Jun Han[2], Wenbo Xu[2], Wenjie Tan[2],

10   Xiaozhong Peng[4], Qi Jin[3], Guizhen Wu[*,2], Chuan Qin[*,1]

11

12   [1] Key Laboratory of Human Disease Comparative Medicine, Chinese Ministry of Health,

13   Beijing Key Laboratory for Animal Models of Emerging and Remerging Infectious

14   Diseases, Institute of Laboratory Animal Science, Chinese Academy of Medical Sciences

15   and Comparative Medicine Center, Peking Union Medical College, Beijing, China.

16   [2] MHC Key Laboratory of Biosafety, National Institute for Viral Disease Control and

17   Prevention, China CDC, Beijing, China.

18   [3] Institute of Pathogen Biology, Chinese Academy of Medical Sciences, Beijing, China.

19   [4] Institute of Medical Biology, Chinese Academy of Medical Sciences, Beijing, China.

20

21   [†]These authors contributed equally to this work.

22   [*]Correspondence should be addressed to Chuan Qin, Email: qinchuan@pumc.edu.cn, or

23   Guizhen Wu, Email: wugz@ivdc.chinacdc.cn.

24 **Abstract**

25 Severe acute respiratory syndrome CoV-2 (SARS-CoV-2) caused the Corona Virus

26 Disease 2019 (COVID-19) cases in China has become a public health emergency of

27 international concern (PHEIC). Based on angiotensin converting enzyme 2 (ACE2) as

28 cell entry receptor of SARS-CoV, we used the hACE2 transgenic mice infected with

29 SARS-CoV-2 to study the pathogenicity of the virus. Weight loss and virus replication in

30 lung were observed in hACE2 mice infected with SARS-CoV-2. The typical

31 histopathology was interstitial pneumonia with infiltration of significant lymphocytes and

32 monocytes in alveolar interstitium, and accumulation of macrophages in alveolar cavities.

33 Viral antigens were observed in the bronchial epithelial cells, alveolar macrophages and

34 alveolar epithelia. The phenomenon was not found in wild type mice with SARS-CoV-2

35 infection. The pathogenicity of SARS-CoV-2 in hACE2 mice was clarified and the

36 Koch's postulates were fulfilled as well, and the mouse model may facilitate the

37 development of therapeutics and vaccines against SARS-CoV-2.

38

39 Key words: SARS-CoV-2, pathogenicity, pneumonia, mouse model, hACE2

40

41

42   In late December of 2019, the coronavirus disease 2019 (COVID-19) caused by severe

43   acute respiratory syndrome CoV-2 (SARS-CoV-2), linked to a seafood market in which

44   exotic animals were also sold and consumed, were identified and reported from Wuhan

45   City, Hubei Province, China[1,2]. The number of confirmed cases has since soared, with

46   almost 78,000 cases reported and over 2,700 deaths as of February 25, 2020 in China[3],

47   and imported cases from travelers of mainland China in several other countries. It is

48   critical to find the pathogenicity and biology of the virus for prevention and treatment of

49   the disease.

50   Because SARS-CoV-2 was highly homologous with severe acute respiratory

51   syndrome coronavirus (SARS-CoV), human angiotensin-converting enzyme 2 (hACE2),

52   which was the entry receptor of SARS-CoV, was also considered to have a high binding

53   ability with the SARS-CoV-2 by molecular biological analysis[4,5]. Therefore, we used the

54   hACE2 transgenic and wild type (WT) mice infected with SARS-CoV-2 to study the

55   pathogenicity of the virus.

56   Specific pathogen-free, 6-11-month-old, male and female WT mice (WT-HB-01,

57   n=15) and hACE2 mice (ACE2-HB-01, n=19) were inoculated intranasally with SARS-

58   CoV-2 stock virus (HB-01) at a dosage of 10^5 $TCID_{50}$/50 μl inoculum volume per mouse

59   after the mice were anesthetized by 2.5% avertin, and the mock-treated hACE2 mice

60   (ACE2-Mock, n=15) were used as control. Clinical manifestations were recorded from

61   thirteen mice (WT-HB-01, n=3; ACE2-Mock, n=3; ACE2-HB-01, n=7). Compared to

62   WT-HB-01 mice and ACE2-Mock mice, slight bristles and weight loss were only

63   observed in ACE2-HB-01 mice during the 14 days observation, and other clinical

64   symptoms such as arched back and decreased projection of external stimuli were not

65 found. Notably, the weight loss of ACE2-HB-01 mice was up to 8% at 5 days post

66 infection (dpi) (Figure 1a).

67   Next, viral replication and pathological changes were examined from three animals

68 per group at each time point, and the primary organs were collected periodically,

69 including heart, liver, spleen, lung, kidney, brain, intestine and testis. As shown in Figure

70 1b, viral loads were detected by qRT-PCR at 1 dpi, 3 dpi, 5 dpi and 7 dpi in the lungs of

71 ACE2-HB-01 mice but not in that of WT-HB-01mice (data not shown), and the viral

72 RNA copies reached a peak at 3 dpi ($10^{6.77}$ copies/ml). Interestingly, the viral RNA was

73 also detected at 1 dpi in the intestine of ACE2-HB-01 mice, which was failed to be

74 detected in other tissues along the timeline (Figure 1b). Consistent to the results of viral

75 loads, infectious virus was respectively isolated from the lungs of ACE2-HB-01 mice at 1

76 dpi, 3 dpi and 5 dpi, and the highest virus titers were detected at 3 dpi ($10^{2.44}$ TCID$_{50}$/100

77 μl) (Figure 1c). Meanwhile, the infectious virus was isolated by Vero E6 cells culture

78 from lung, and the SARS-CoV-2 particles were observed by electron microscopy (Figure

79 1d). However, the virus was failed to be isolated from the lungs in WT-HB-01 mice and

80 ACE2-Mock mice along the detecting timeline (Figure 1c), which suggested that hACE2

81 was essential for SARS-CoV-2 infection and replication in mice. Moreover, specific IgG

82 antibodies against S protein of SARS-CoV-2 were positively measured in the sera of

83 ACE2-HB-01 mice at 21 dpi (Figure 1e).

84   There were no obviously gross and histopathological changes at 1 dpi in all the

85 animals of each group. Compared to WT-HB-01 mice or ACE2-mock mice with

86 homogeneously pink and slightly deflated, all the ACE2-HB-01 mice at 3 dpi displayed

87 comparable gross lesions with focal to multifocal dark red discoloration in certain lung

88 lobes. The lesions progressed into multifocal to coalescent scattered-dark reddish purple

89 areas and focal palpable nodules throughout the lung lobes at 5 dpi (Figure 2a). The

90 damaged lungs became swollen and enlarged in size. Microscopically, consistently, lung

91 tissues from ACE2-HB-01 mice at 3 dpi showed moderate, multifocal, interstitial

92 pneumonia. Inflammatory cells including lymphocytes and monocytes accumulated in the

93 alveolar interstitium and caused thickening of the alveolar walls (Figure 2a). Increased

94 collagen fiber in the thickened alveolar interstitium in the ACE2-HB-01 mice was

95 confirmed by Modified Masson's Trichrome stain with blue colors (Supplementary

96 Figure 1a). The bronchiolar epithelial cells showed swelling, degeneration, some of

97 which dissolved (Figure 2a). Affected bronchioles were filled with occasionally small

98 amounts of periodic acid-Schiff (PAS) positive-exudation or denatured and detached

99 bronchiolar epithelium (Supplementary Figure 1b). The alveolar cavities were dispersed

100 mainly by swollen and degenerative alveolar macrophages and lymphocytes (Figure 2a).

101 To investigate the infiltration of specific inflammatory cells, immunohistochemical (IHC)

102 was carried out to identify MAC2$^+$ macrophages (Supplementary Figure 2a), CD3$^+$ T

103 lymphocytes, and CD19$^+$ B lymphocytes (Supplementary Figure 2b). Compared to the

104 WT-HB-01 mice, more macrophages, T lymphocytes, and B lymphocytes were observed

105 in the lungs of ACE2-HB-01 mice along with lasting prolonged infection time. The

106 MAC2$^+$ macrophages were diffusely infiltrated in the alveolar cavities (at 3 dpi) or

107 focally aggregated together in the thickened alveolar septum (at 5 dpi, Supplementary

108 Figure 2a). CD3$^+$ T lymphocytes and CD19$^+$ B lymphocytes were scattered dispersed or

109 occasionally aggregated in the alveolar interstitium in the ACE2-HB-01 mice, by contrast,

110 they were rarely observed in the WT-HB-01 mice (Supplementary Figure 2b).

111   Perivascular infiltrated inflammatory cells, including lymphocytes and monocytes, were

112   observed multifocally within and adjacent to affected areas of the lungs. At 5 dpi, the

113   lung progressed into coalescing interstitial pneumonia with diffuse lesions. Thickened

114   alveolar septa were filled with lymphocytes and monocytes (Figure 2a). IHC staining of

115   sequential section revealed that viral antigens were found in the alveolar macrophages,

116   alveolar epithelia, and the degenerative and being desquamated bronchial epithelial cells

117   (Figure 2b). There were no significant histopathological lesions (Supplementary Figure 3)

118   or viral antigens of SARS-CoV-2 (Supplementary Figure 4) in the other organs, including

119   myocardium, liver, spleen, kidney, cerebrum, intestine, and testis. At 7 dpi, the

120   pneumonia became mild with focal lesion areas (data not shown).

121   In addition, the co-localization of SARS-CoV-2 S protein (Fifure 3f) and hACE2

122   receptor (Figure 3g) was demonstrated in alveolar epithelial cells of ACE2-HB-01 mice

123   by immunofluorescence (Figures 3h). The phenomenon was not found in the ACE2-

124   Mock mice (Figures 3a, b, c and d) or WT-HB-01 mice (data not shown), indicating that

125   the SARS-CoV-2, as same as SARS-CoV, also utilizes the hACE2 as a receptor for

126   entry[4].

127   The speed of geographical spread of COVID-19 caused by SARS-CoV-2 has been

128   declared as public health emergency of international concern (PHEIC), with cases

129   reported on multiple continents only weeks after the disease was first reported[6]. Although

130   it has been determined by bioinformatics that the pathogen of this epidemic is a novel

131   coronavirus, it is necessary to be confirmed by animal experiments following Koch's

132   postulates.

133   In the present study, after the experimental infection of hACE2 transgenic mice with

134   one of the earliest known isolates of SARS-CoV-2, the mice lost weight and showed

135   interstitial pneumonia, which are comparable with initial clinical reports of pneumonia

136   caused by SARS-CoV-2[7]. Meanwhile, virus replication was detected in the lung of

137   ACE2-HB-01 mice and elicited the specific IgG against SARS-CoV-2. In clinical

138   autopsy, histological examination showed bilateral diffuse alveolar damage with cellular

139   fibromyxoid exudates[8]. Correspondingly, ACE2-HB-01 mice showed coalescing

140   interstitial pneumonia in this study. Furthermore, specifically histopathology changes and

141   progress were observed in the mice, e.g. affected bronchioles were filled with

142   occasionally small amounts of periodic acid schiff (PAS) positive-exudation or denatured

143   and detached brochiolar epithelium.

144   The case fatality rate of currently reported cases is about 2%, which implies that so

145   far, this novel coronavirus does not seem to cause the high fatality rates as SARS-CoV

146   (9-11%)[9], which suggested the difference in pathogenicity between the two viruses. The

147   pathogenicity of SARS-CoV-2 seems mild compared to SARS-CoV in mice, the latter

148   caused extrapulmonary organ damage, includes brain, kidney, intestine, heart and liver,

149   furthermore, the neurons are susceptible for SARS-CoV infection, and cerebral casculitis

150   and hemorrhage were observed in hACE2 transgenic mice[10,11]. However, only interstitial

151   pneumonia was observed in SARS-CoV-2-infected hACE2 mice, implying the disparity

152   in pathogenicity of the coronavirus.

153   Therefore, our results clarified the pathogenicity of SARS-CoV-2 in mice, together

154   with the previous clinical studies[7], completely fulfills the Koch's postulates[12] and

155 confirmed SARS-CoV-2 was the pathogen of COVID-19. The mouse model may

156 facilitate the development of therapeutics and vaccines against SARS-CoV-2.

157

158 **Materials and methods**

159 *Ethics statement*

160 Murine studies were performed in an animal biosafety level 3 (ABSL3) facility using

161 HEPA-filtered isolators. All procedures in this study involving animals were reviewed

162 and approved by the Institutional Animal Care and Use Committee of the Institute of

163 Laboratory Animal Science, Peking Union Medical College (BLL20001).

164

165 *Viruses and cells*

166 The SARS-CoV-2 (strain HB-01) was kindly provided by Professor Wenjie Tan[1], from

167 the China Centers for Disease Control and Prevention (China CDC). The complete

168 genome for this SARS-CoV-2 was submitted to GISAID (BetaCoV/Wuhan/IVDC-HB-

169 01/2020|EPI_ISL_402119), and deposited in the China National Microbiological Data

170 Center (accession number NMDC10013001 and genome accession numbers

171 MDC60013002-01). Seed SARS-CoV-2 stocks and virus isolation studies were

172 performed in Vero cells, which are maintained in Dulbecco's modified Eagle's medium

173 (DMEM, Invitrogen, Carlsbad, USA) supplemented with 10% fetal bovine serum (FBS),

174 100 IU/ml penicillin, and 100 µg/ml streptomycin, and incubated at 37°C, 5% CO_2. For

175 infected mice, the lung homogenates were used for virus titration tests using endpoint

176 titration in Vero E6 cells. Virus titer of the supernatant were determined using a standard

177 50% tissue culture infection dose (TCID50) assay.

178

179 *Animal experiments*

180 For the animal experiments, specific pathogen-free, 6-11-month-old, male and female

181 transgenic hACE2 mice were obtained from the Institute of Laboratory Animal Science,

182 Peking Union Medical College, China. Transgenic mice were generated by

183 microinjection of the mice ACE2 promoter driving the human ACE2 coding sequence

184 into the pronuclei of fertilized ova from ICR mice, and then human ACE2 integrated was

185 identified by PCR as previous described[10], the hACE2 mainly expressed in lung, heart,

186 kidney, and intestine of transgenic mice. The hACE2 mice or WT (ICR) mice were

187 respectively inoculated intranasally with SARS-CoV-2 stock virus at a dosage of 10^5

188 $TCID_{50}$ and hACE2 mice intranasally inoculated with equal volume of PBS was used as

189 mock-infection control. The infected animals were continuously observed daily to record

190 body weights, clinical symptoms, responsiveness to external stimuli and death. And the

191 mice were dissected at 1 dpi 3 dpi, 5 dpi and 7 dpi respectively to collect different tissues

192 to screen virus replication and histopathological changes.

193

194 *Preparation of Homogenate Supernatant*

195 Tissues homogenates were prepared by homogenizing perfused whole tissue using an

196 electric homogenizer for 2 min 30 s in 1 ml of DMEM. The homogenates were

197 centrifuged at 3,000 rpm for 10 min at 4°C. The supernatant was collected and stored at

198 −80°C for viral isolation and viral load detection.

199

200 *RNA extraction and qRT-PCR*

201   Total RNA was extracted from organs using the RNeasy Mini Kit (Qiagen, Hilden,

202   Germany), and reverse transcription was performed using the PrimerScript RT Reagent

203   Kit (TaKaRa, Japan) following manufacturer instructions. A quantitative real-time

204   reverse transcription-PCR (qRT-PCR) reactions were performed using the PowerUp

205   SYBG Green Master Mix Kit (Applied Biosystems, USA), in which samples were

206   processed in duplicate using the following cycling protocol: 50°C for 2 min, 95°C for 2

207   min, followed by 40 cycles at 95°C for 15 s and 60°C for 30 s, and then 95°C for 15 s,

208   60°C for 1 min, 95°C for 45 s. The primer sequences used for RT-PCR are targeted

209   against the envelope (E) gene of SARS-CoV-2 and are as follows: Forward: 5'-

210   TCGTTTCGGAAGAGACAGGT-3', Reverse: 5'-GCGCAGTAAGGATGGCTAGT-3'.

211   The PCR products were verified by sequencing using the dideoxy method on an ABI

212   3730 DNA sequencer (Applied Biosystems, CA, USA). During the sequencing process,

213   amplification was performed using specific primers. The sequences for this process are

214   available upon request. The sequencing reads obtained were linked using DNAMAN, and

215   the results were compared using the Megalign module in the DNAStar software package.

216

217   *ELISA method*

218   The specific IgG against SARS-CoV from ACE2-HB-01 mice and WT-HB-01 mice were

219   determined by enzyme-linked immunosorbent assay (ELISA). 96-well plates were coated

220   with Spike 1 protein of SARS-CoV-2 (0.1μg/100 μL, Sino Biological, 40591-V08H), the

221   tested sera were diluted at 1:100 and added to each well, and 3 multiple wells were set for

222   each sample, and then incubated at 37℃ for 30 minutes, followed by the goat anti-mouse

223   secondary antibodies conjugated with HRP (ZB-2305, zhongshan,1:10,000 dilution), and

224   incubated at room temperature for 30 minutes. The reaction was developed by TMB

225   substrate and the optical densities at 450 nm were determined (Metertech960 enzyme

226   marker with 450 nm wavelength).

227

228   *Laboratory preparation of the antibody of SARS-CoV-2 Spike-1 (S1) protein*

229   Mice were immunized with purified SARS-CoV-2 S1 protein (Sino biological) and

230   splenocytes of hyper immunized mice were fused with myeloma cells. Positive clones

231   were selected by ELISA using SARS-CoV-2 S1 protein (Supplementary Figure 1). The

232   cell supernatant of 7D2 clone, binding to SARS-CoV-2 S1 protein, was collected for

233   immunofluorescence analysis.

234

235   *Pathological Examination*

236   Autopsies were performed in the animal biosafety level 3 (ABSL3) laboratory. Major

237   organs were grossly examined and then fixed in 10% buffered formalin solution, and

238   paraffin sections (3-4 µm in thickness) were prepared routinely. Hematoxylin and Eosin

239   (H&E) stain, periodic acid-Schiff (PAS) stain and modified Masson's Trichrome stain

240   were used to identify histopathological changes in all the organs. The histopathology of

241   the lung tissue was observed by light microscopy.

242

243   *Immunohistochemistry (IHC)*

244   The organs were fixed in 10% buffered formalin solution, and paraffin sections (3-4 µm

245   in thickness) were prepared routinely. Sections were treated with an antigen retrieval kit

246   (Boster, AR0022) for 1 min at 37℃ and quenched for endogenous peroxidases in 3%

247   H_2O_2 in methanol for 10 min. After blocking in 1% normal goat serum, the sections were

248   incubated with 7D2 monoclonal antibody (laboratory preparation) at 4℃ overnight,

249   followed by HRP-labeled goat anti-mouse IgG secondary antibody (HRP) (Beijing ZSGB

250   Biotechnology, ZDR-5307). Alternatively, the sections were stained with MAC2

251   antibody (Cedarlane Laboratories, CL8942AP), CD3 antibody (Dako, A0452) or CD19

252   antibody (Cell Signaling Technology, 3574) at 4℃ overnight. Subsequently, the sections

253   were goat anti-rat IgG secondary antibody (HRP) (Beijing ZSGB Biotechnology,

254   PV9004), goat anti-rabbit IgG secondary antibody (HRP) (Beijing ZSGB Biotechnology,

255   PV9001) for 60 min, and visualized by incubation with 3,30-diaminobenzidine

256   tetrahydrochloride (DAB). The slices were counterstained with hematoxylin, dehydrated

257   and mounted on a slide and viewed under an Olympus microscope.

258

259   *Confocal microscopy*

260   For viruses and hACE2 receptor co-localization analysis, the lung tissue sections were

261   washed twice with PBS, fixed by Immunol Staining Fix Solution (P0098), blocked 1 hour

262   at room temperature by Immunol Staining Blocking Buffer (P0102) and then incubated

263   overnight at 4°C with the appropriate primary and secondary antibodies. The nuclei were

264   stained with DAPI. Anti-S protein antibody (mouse monoclonal 7D2, laboratory

265   preparation, 1:200) and anti-hACE2 antibody (rabbit polyclonal, ab15348, Abcam1:200)

266   were used as the primary antibody. The sections were washed with PBS and incubated

267   with secondary antibodies conjugated with FITC (goat anti-mouse, ZF-0312, Beijing

268   ZSGB Biotechnology, 1:200) and TRITC (goat anti rabbit, ZF-0317, Beijing ZSGB

269   Biotechnology, 1:200), dried at room temperature and observed via fluorescence

270   microscopy. For the expression of hACE2, the sections from WT mice stained with anti-

271   ACE2 antibody were used as the negative control, and the stable cell line expressing

272   hACE2 was used as the positive control. For the viral antigen, the sections from ACE2-

273   Mock mice incubated with anti-S protein antibody were used as the negative control.

274

275   *Transmission Electron Microscopy*

276   Supernatant from Vero E6 cell cultures that showed cytopathic effects was collected,

277   inactivated with 2% paraformaldehyde for at least 2 hours, and ultracentrifuged to

278   sediment virus particles. The enriched supernatant was negatively stained on film-coated

279   grids for examination. The negative stained grids were observed under transmission

280   electron microscopy.

281

282   *Statistical analysis*

283   All data were analyzed with GraphPad Prism 8.0 software. Statistically significant

284   differences between two groups were determined using unpaired Student's *t*-tests. The

285   statistical significance among three groups was assessed by one-way ANOVA. A two-

286   sided p value<0.05 was considered statistically significant.

287

288   **Acknowledgement**

289   We thank Dr George F Gao for his advice and coordination on this work. We thank

290   Hongkui Deng, Xiuhong Yang and Lianfeng Zhang for providing the hACE2 mice as a

291   gift. We also thank Gary Wong for helping us proofread the language. This work was

299   **References**

300   1   Zhu, N. *et al.* A Novel Coronavirus from Patients with Pneumonia in China, 2019. *N Engl J*
301   *Med*, 10.1056/NEJMoa2001017, doi:10.1056/NEJMoa2001017 (2020).
302   2   Ren, L. L. *et al.* Identification of a novel coronavirus causing severe pneumonia in human:
303   a descriptive study. *Chinese medical journal*, doi:10.1097/cm9.0000000000000722
304   (2020).
305   3   Commission, C. N. H. *Update on the novel coronavirus pneumonia outbreak (Jan 24,*
306   *2020).   Beijing: China   National   Health   Commission,   2020,   <*
307   http://www.nhc.gov.cn/yjb/s7860/202002/84faf71e096446fdb1ae44939ba5c528.shtml>
308   (2020).
309   4   Xu, X. *et al.* Evolution of the novel coronavirus from the ongoing Wuhan outbreak and
310   modeling of its spike protein for risk of human transmission. *Science China. Life sciences*,
311   doi:10.1007/s11427-020-1637-5 (2020).
312   5   Kuba, K. *et al.* A crucial role of angiotensin converting enzyme 2 (ACE2) in SARS
313   coronavirus–induced lung injury. *Nature Medicine* **11**, 875-879, doi:10.1038/nm1267
314   (2005).
315   6   Chan, J. F. *et al.* A familial cluster of pneumonia associated with the 2019 novel
316   coronavirus indicating person-to-person transmission: a study of a family cluster. *Lancet*
317   **395**, 514-523, doi:10.1016/s0140-6736(20)30154-9 (2020).
318   7   Huang, C. *et al.* Clinical features of patients infected with 2019 novel coronavirus in
319   Wuhan, China. *Lancet* **395**, 497-506, doi:10.1016/s0140-6736(20)30183-5 (2020).
320   8   Xu, Z. *et al.* Pathological findings of COVID-19 associated with acute respiratory distress
321   syndrome. *The Lancet. Respiratory medicine*, doi:10.1016/s2213-2600(20)30076-x
322   (2020).
323   9   de Wit, E., van Doremalen, N., Falzarano, D. & Munster, V. J. SARS and MERS: recent
324   insights into emerging coronaviruses. *Nature reviews. Microbiology* **14**, 523-534,
325   doi:10.1038/nrmicro.2016.81 (2016).
326   10   Yang, X. H. *et al.* Mice transgenic for human angiotensin-converting enzyme 2 provide a
327   model for SARS coronavirus infection. *Comparative medicine* **57**, 450-459 (2007).
328   11   Netland, J., Meyerholz, D. K., Moore, S., Cassell, M. & Perlman, S. Severe acute
329   respiratory syndrome coronavirus infection causes neuronal death in the absence of
330   encephalitis in mice transgenic for human ACE2. *J Virol* **82**, 7264-7275,
331   doi:10.1128/jvi.00737-08 (2008).
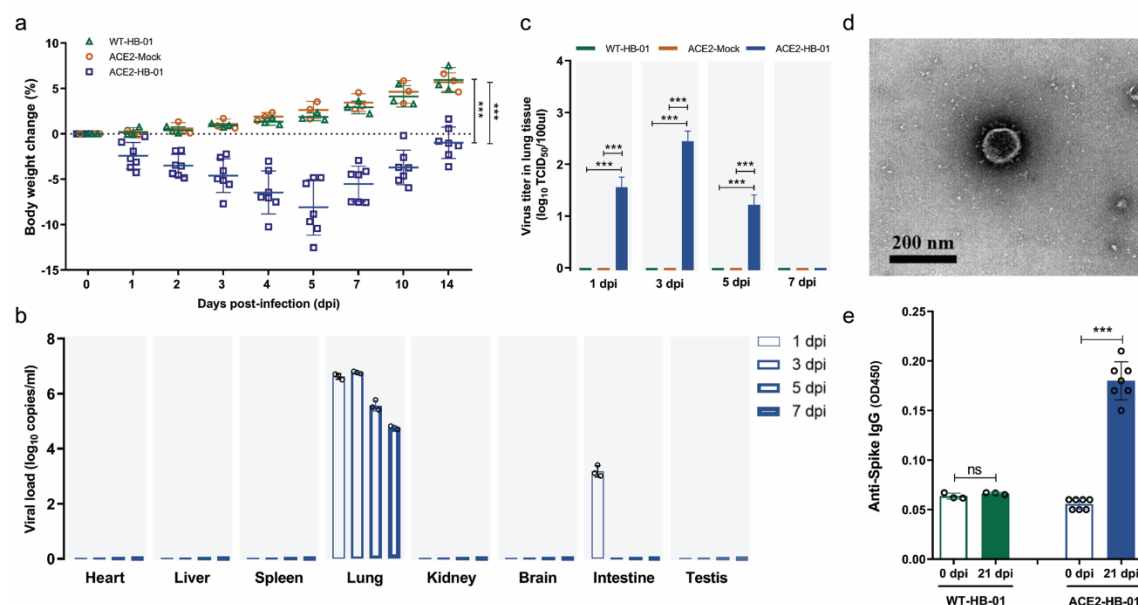332   12   Rivers, T. M. Viruses and Koch's Postulates. *Journal of bacteriology* **33**, 1-12 (1937).

Figure 1. Weight loss, virus replication and specific IgG production in hACE2 mice post infection with SARS-CoV-2. For weigh loss record, hACE2 mice (n=7) and WT mice (n=3) were experimentally challenged intranasally with SARS-CoV-2, and the ACE2-Mock mice (n=3) were used as control. And then the weight loss was recorded over 14 days (a, ANOVA, ***$p<0.001$*). To screen virus replication, 12 mice were infected in each group, and 3 mice per group were sacrificed and their major organs harvested for viral load and virus titer at 1 dpi, 3 dpi, 5 dpi and 7 dpi respectively. The distribution of SARS-CoV-2 in the primary organs of ACE2-HB-01 mice was detected by qRT-PCR (b). Virus titers of lungs were determined on Vero E6 cells (c, unpaired *t*-test, ***$p<0.001$*), and the virus isolated from lungs of ACE2-HB-01 mice at 3 dpi was observed by electron microscope (d). The specific IgG against SARS-CoV-2 was detected at 21 dpi by ELISA (e, unpaired *t*-test, ***$p<0.001$*).
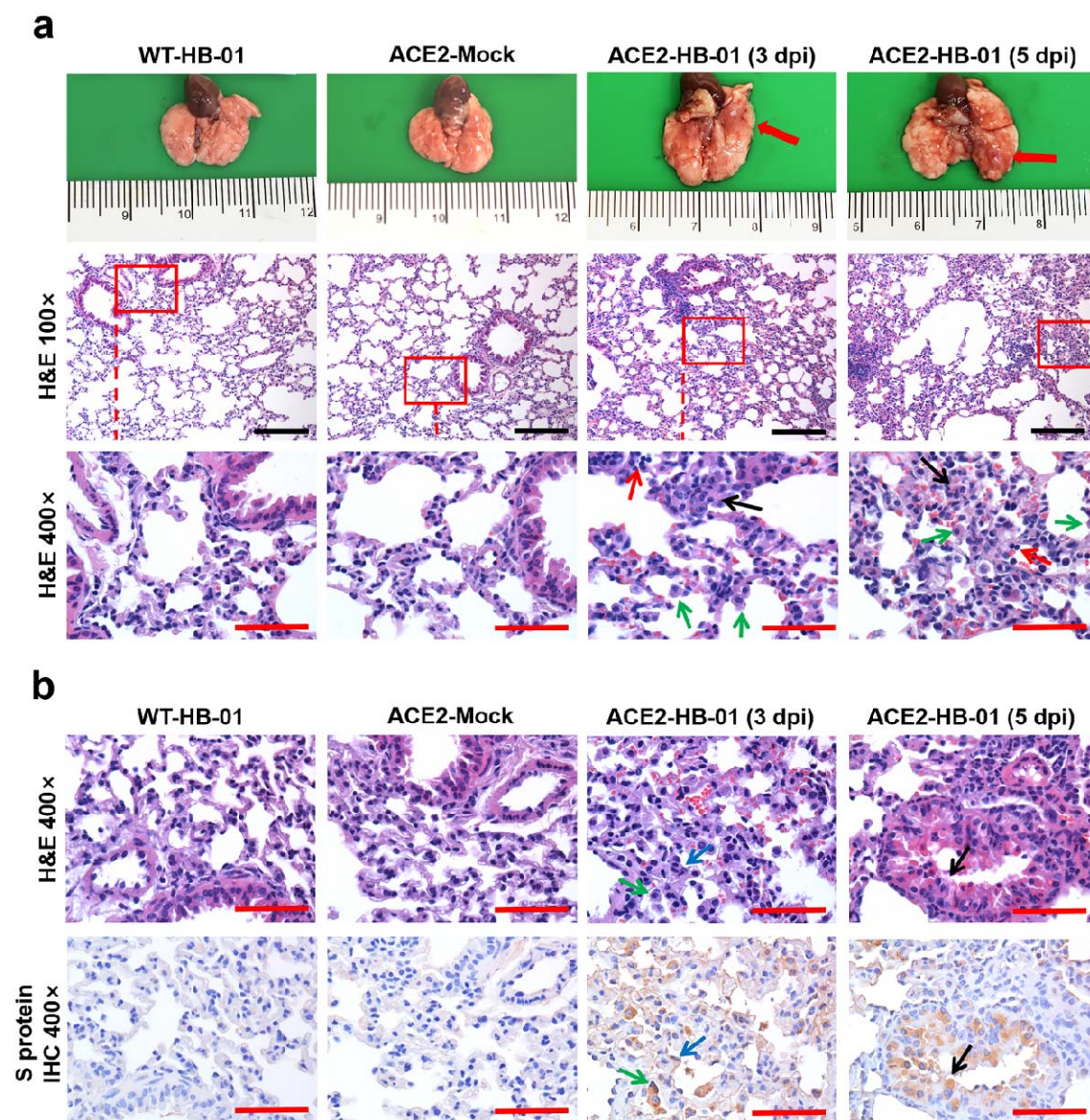
Figure 2. Gross pathology, histopathology, and immunohistochemistry of the lungs in SARS-CoV-2-infected hACE2 mice. a. Gross pathology and histopathology of lungs from WT-HB-01 mice (3 dpi), ACE2-Mock mice (3 dpi) and ACE2-HB-01 mice (3 dpi and 5 dpi). Postmortem examinations showed focal dark red lesions (red arrow) throughout the dorsal of the right middle lobe of the lung at 3dpi. The lesions progressed into multifocally scattered-dark reddish purple areas and palpable nodules (red arrow) throughout the right lobe of the lung at 5 dpi. Histopathological observation indicated that

355   moderate interstitial pneumonia with thickened alveolar septa (black arrows) and

356   infiltration of lymphocytes (red arrows). The swollen and degenerative alveolar

357   macrophages (green arrows) are scattered within the alveolar cavities at 3dpi and 5 dpi. b.

358   Immunohistochemical examination of lungs of each group. The sequential sections were

359   stained by HE and IHC, respectively. The viral antigens were observed in the alveolar

360   macrophage (green arrows), the alveolar epithelia (blue arrows), and the degenerative and

361   being desquamated bronchial epithelial cells (black arrows). Black bar = 100 µm, red bar

362   = 50 µm.

363
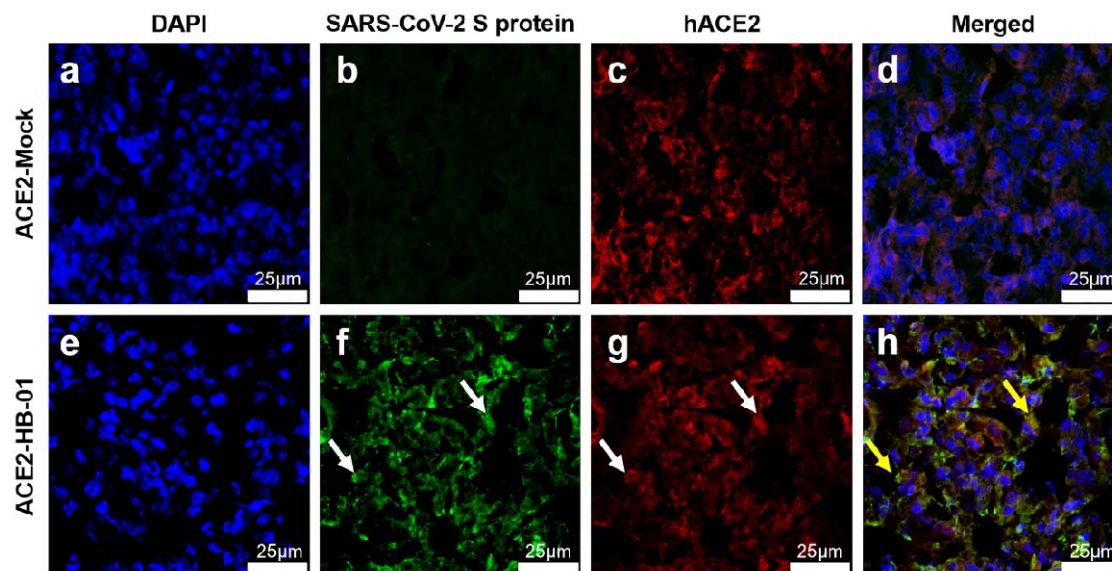
Figure 3. Immunofluorescence analysis of viral antigens in lungs of SARS-CoV-2-infected hACE2 mice. Co-localization of SARS-CoV-2 S protein and hACE2 receptor in hACE2 mouse lungs, the sections were incubated with anti-SARS-CoV-2 S protein antibody, anti-human ACE2 antibody, and DAPI. The lung sections of ACE2-Mock mice (a-d). The lung sections of ACE2-HB-01 mice (e-h). The white arrows showed the viral S protein (f) and hACE2 (g), respectively, the yellow arrow showed the merge of viral S protein and hACE2 (h). White bar=25 µm.
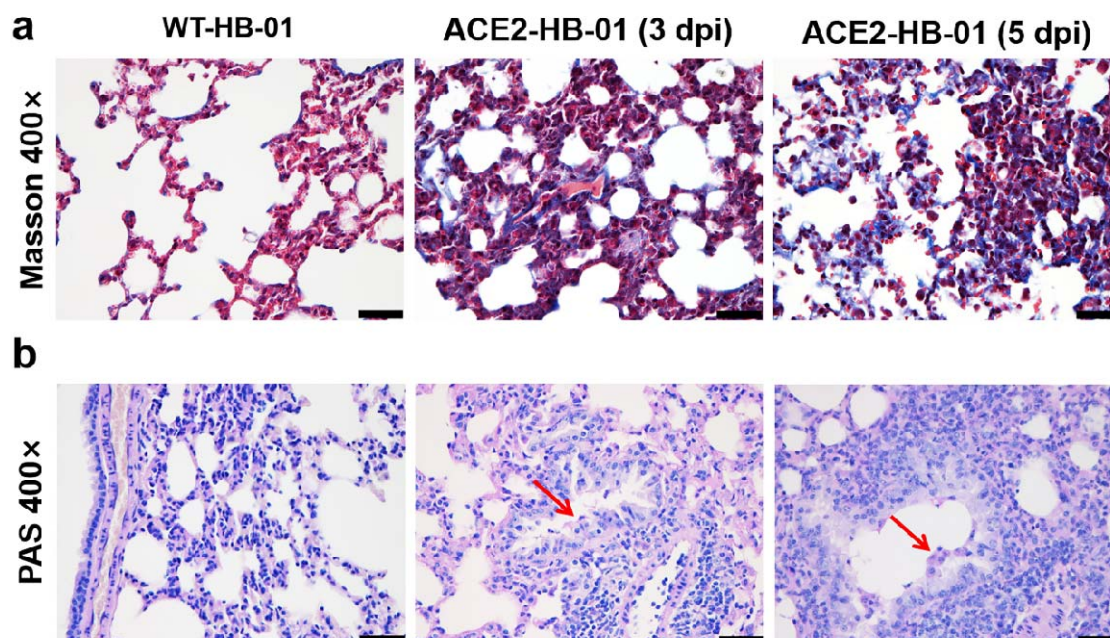
Supplementary Figure 1. Special stains of the lungs in the WT-HB-01 and ACE2-HB-01 mice at 3dpi and 5 dpi. a. Modified Masson's Trichrome of the lung. Compared to the WT-HB-01 group, the increased collagen fiber (blue-stained fibers) in the thickened alveolar interstitium were observed in both the ACE2-HB-01 mice at 3dpi and 5 dpi. b. Periodic acid schiff (PAS) staining of the respiratory epithelium in bronchioles. A small amount of mucus was accumulated on the surface of bronchial epithelial cells. Black bar=40 μm.

382
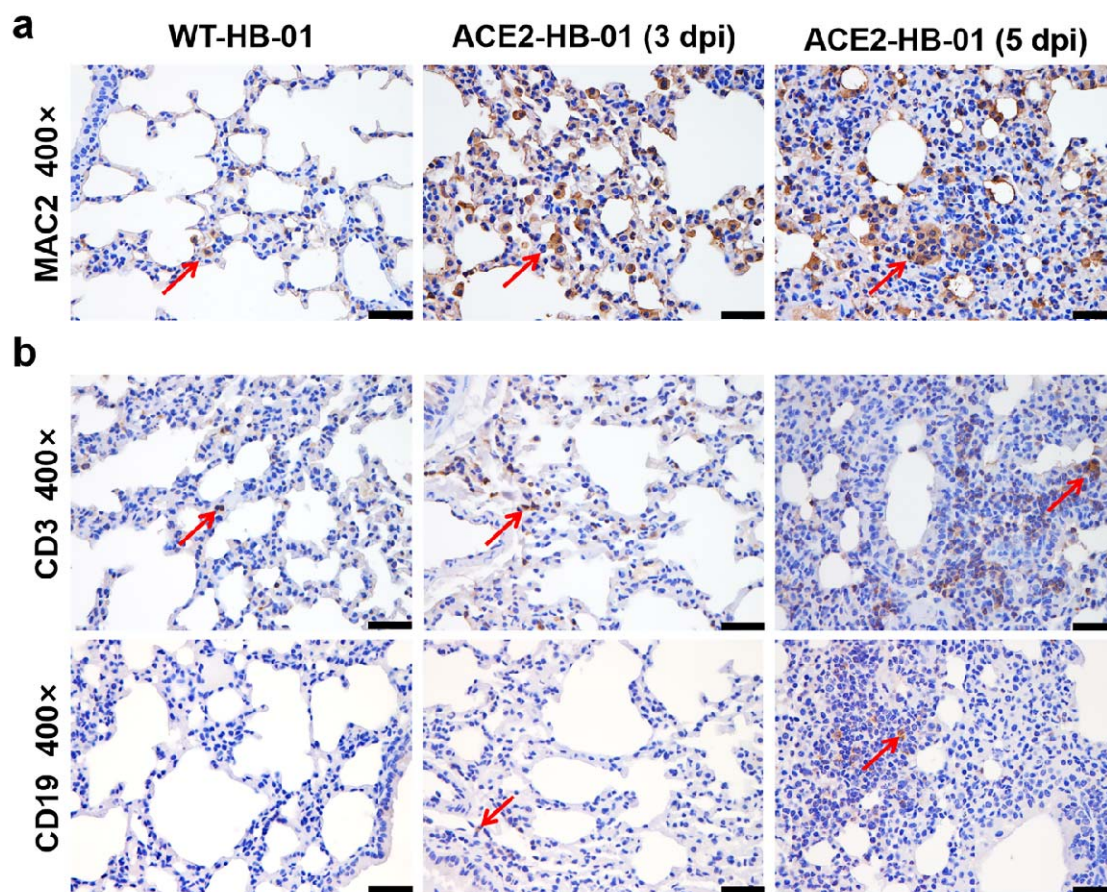
Supplementary Figure 2. IHC was carried out to identify macrophages with MAC2, T lymphocytes with CD3, and B lymphocytes with CD19. a. Diffuse infiltration of macrophages (red arrow) in the expanded alveolar septum in the ACE2-HB-01 mice at 3 dpi and 5 dpi. b. Many T lymphocytes (red arrow) infiltrated the thickened alveolar septa in the first row of b at 5 dpi in the ACE2-HB-01 mice. A few B lymphocytes (red arrow) were observed in the ACE2-HB-01 mice. Black bar=40 μm.

389

390
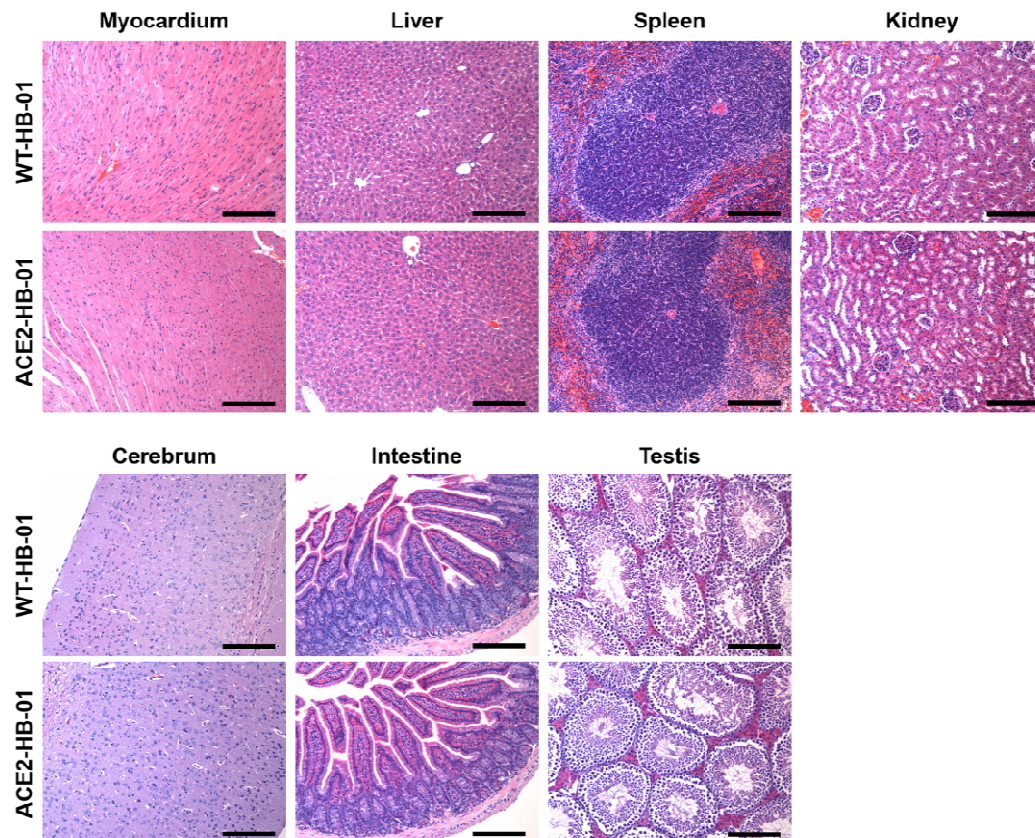
Supplementary Figure 3. The histopathological observation of the organs in the WT-HB-01 and ACE2-HB-01 mice. There were no significant histopathological lesions in the organs, including myocardium, liver, spleen, kidney, cerebrum, intestine and testis in the ACE2-HB-01 mice compared with the ACE2-Mock mice. Black bar = 100 µm.

395
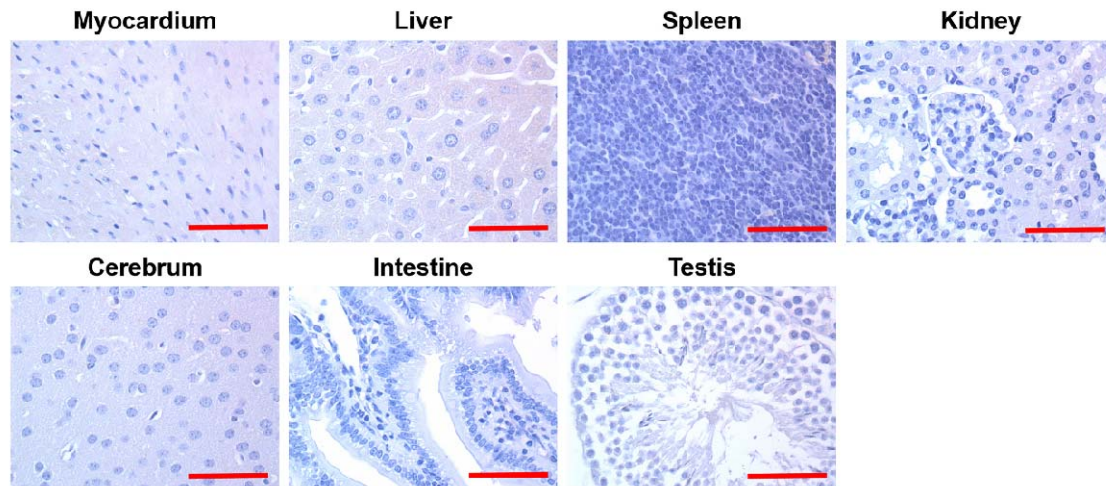
Supplementary Figure 4. The immunohistochemical (IHC) observation of the organs in the ACE2-HB-01 mice. There were no SARS-CoV-2 antigens in the organs, including myocardium, liver, spleen, kidney, cerebrum, intestine and testis. Red bar = 50 µm.

402
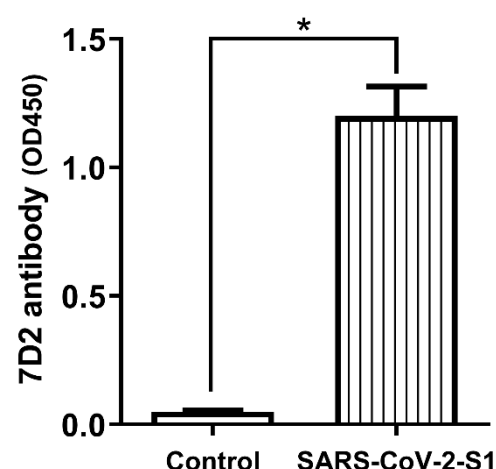
Supplementary Figure 5. Identification of 7D2 antibody against SARS-CoV-2 S1 protein. The plate coated by 0.2 ug SARS-CoV-2 S1 protein was incubated with 7D2 antibody as primary antibody (1:200) and detected using HRP-conjugated goat anti-mouse secondary antibody. The titer of antibody was determined using enzyme-linked immunosorbent assay (ELISA) assay. Significant differences are indicated with an asterisk (unpaired *t*-test, *$p<0.05$).

403
404
405
406
407
408
409
410
411
412